Kovove Mater. 54 2016 463–470
DOI: 10.4149/km_2016_6_463

Effects of chemical composition on the pore structure and heat treatment on the deformation of PM aluminium foams 6061 and 7075

Ľ. Orovčík[1,2]*, M. Nosko[1], J. Kováčik[1], T. Dvorák[1], M. Štěpánek[1,2], F. Simančík[1]

[1] *Institute of Materials and Machine Mechanics, Slovak Academy of Sciences, Dúbravská cesta 9, 845 13 Bratislava 4, Slovak Republic*
[2] *Institute of Materials Science, Faculty of Materials Science and Technology in Trnava, Slovak University of Technology in Bratislava, Paulínska 16, 917 24 Trnava, Slovak Republic*

Received 19 May 2016, received in revised form 26 September 2016, accepted 27 September 2016

Abstract

In this paper we consider deformation behaviour and energy absorption ability of the heat-treated aluminium foams AA6061 and AA7075 with respect to variability of pore structure and defects in cell wall affected by the chemical composition of the foamable precursor itself. The work was focused on the evaluation of cell wall microstructure, the geometry of pores and defects present within the cell walls, and their influence on strength and deformation behaviour properties of the foam.

K e y w o r d s: aluminium foam, heat treatment, compression strength, compression behaviour, reproducibility

1. Introduction

The porous structure of closed cell aluminium foams offers the ability to absorb kinetic energy at nearly constant stress in wide deformation range [1–5]. Aluminium foams made via the powder metallurgical route (PM) with surface skin have better mechanical properties like compression strength than open-cell aluminium foam, and aluminium foam prepared via melting route [2–4, 6–8]. Therefore PM aluminium foam is more recommended for industrial and automotive applications, as it is possible very effectively to produce 3D complex shape parts which led to first industrial applications (developed at IMMM SAS, Bratislava) of PM aluminium foams in Ferrari Modena 360 (stiffener of side rail, 6,000 pcs year^{-1}), Audi Q7 (crash box against rare impact, 120,000 pcs year^{-1}) and Siemens and Bombardier light trains (bumper of railway carriages, 1,000 pcs year^{-1}) [9]. Based on the requirements of industry and industrial applications, it is necessary to develop materials for deformation purposes where it is possible to influence the compression strength and the length of the plateau. Compression strength of foams is affected by material composition, heat treatment [10–13], by the deployment of the precursor into a mould and amount of precursor [8], foam density, pore size and their distribution within the structure and close to surface skin [8, 14–18]. Effect of heat treatment on compression strength of AA 6061 aluminium foam has been described in several studies [10–13, 19]. AA6061 deforms in a ductile manner, whereas AA7075 is brittle in nature. Subsequent T6 treatment changes the deformation behaviour of AA6061 from ductile to brittle [10, 19–23]. Effect of different chemical composition and ways of heat treatment of AA7XXX on compression strength and absorption ability was studied and also fracture surface of cell walls before and after heat treatment of aluminium foam was observed [11, 23]. The stress-strain behaviour of foams is very sensitive and determined by the properties of the cell wall material: hardness, strength, the thickness of cell walls and surface skin [7, 8, 17, 18, 23].

Moreover, defects in cell walls like microcracks, micropores, corrugations of cell walls and inhomogeneities of chemical composition have also a strong

*Corresponding author: tel.: +421 2 3240 1042; e-mail address: lubomir.orovcik@savba.sk

effect on the compression strength and deformation behaviour of the foam at given porosity and pore structure. Until now, the origin of the brittle disintegration of the foam structure during compression has not been described concerning defects within cell walls and their character. Therefore, the aim of this work is to observe an effect of the chemical composition of AA6061 and predominantly AA7075 PM aluminium alloys and their heat treatment on the foam structure and microstructure of cell walls, mainly the effect on the deformation behaviour and energy absorption ability.

2. Experimental

The foamable precursor was manufactured through PM route by mixing the pure elementary powders and pre-alloyed Al + 5 wt.% Mg powder which was used to adjust the Mg content. The chemical composition of mixed alloy corresponded to the EN AW 6061 (Al + 1 wt.% Mg + 0.6 wt.% Si) and EN AW 7075 (Al + 2.5 wt.% Mg + 6 wt.% Zn + 2wt.% Cu). For manufacturing of the foamable precursor, powders were used: Al powder (99.7 % purity; $< 400\,\mu m$), supplied by Eckart (Germany); pre-alloyed AlMg5 powder (99.7 % purity; $< 400\,\mu m$), Zn (98.9 % purity; $< 100\,\mu m$) and Si (99.9 % purity; $< 40\,\mu m$) were supplied by Mepura (Austria); Cu (99.8 % purity; $< 100\,\mu m$) was supplied by Chempur (Germany). Amount of 0.8 wt.% of foaming agent TiH_2 from Chemetall (Germany), (grade U, nominally $\leq 45\,\mu m$, average particle size $d = 5 \pm 1\,\mu m$) was admixed with each powder mixture. Afterwards, the final mixtures were cold isostatically compacted (under the pressure of 55 MPa) into billets with a dimension of approximately 30 mm in diameter. Subsequently, they were hot extruded into the profile of the rectangular cross-section $5 \times 20\,mm^2$. The extrusion temperature was set to 450 ℃ for AA6061 and 400 ℃ for AA7075. Since AA7075 contains Zn which melting temperature is 419.53 ℃, heated time for billets was also shorter to minimise oxidation processes. Expandometer testing machine (IMMM SAS, Slovakia) was used to find appropriate temperatures of foaming process. It was found that the temperature of foam nucleation for samples AA6061 was between 580 to 605 ℃ and for samples AA7075 between 470 to 500 ℃. Therefore furnace temperature for sample preparation was set for AA6061 to 730 ℃ and for AA7075 to 700 ℃. Foamed cylinders of diameter 30 mm and length 45 mm with density $\sim 0.6\,g\,cm^{-3}$ were manufactured for each chemical composition. To obtain statistically valuable data, the quantity of foamable precursor and its position within the mould is necessary to control thoroughly [8]. Therefore, mould filling was in both cases held at 42 % and 5 pieces of the foamable precursor were deployed into the mould in the same orientation for all samples. Heat treatment of foamed samples T6 with respect to alloy composition was chosen as follows: Quenching conditions in the case of AA6061 were 530 ℃/30 min and for AA7075 460 ℃/120 min, ageing 170 ℃/12 h in the case of AA6061 and 120 ℃/16 h for AA7075. To reveal the 3-D porous structure of the foam after foaming, a non-destructive 3-D computed tomography was performed using Nanotom 180 GE X-ray tomography. The thickness of cell walls and surface skin at the top, middle and bottom of samples was determined through the VG Studio MAX 2.1 software. The thickness of surface skin was measured around the sample in the area with big pores. Pore size and shape factor (roundness of pores) were determined from 4 slices at 0°, 45°, 90° and 135° through the Image J software. The roundness of pores is taken as the inverse of Aspect Ratio, i.e. the ratio of pore's fitted ellipse minor axis to major axis of the ellipse. The shape of pores was measured on slices by Feret diameter. To observe the distribution of elements and defects in cell walls, images were taken through scanning electron microscope (SEM) JEOL JSM-7600. An effect of the heat treatment on the microhardness of the cell walls was determined using Vickers method on FM-ARS-9000 device. The samples were loaded by 0.049 N (5 g) for 10 s. Compression strength of the foam samples was measured via uniaxial compression tests according to DIN 50134 [24]. The static compression stress (CS) tests were performed on a Zwick testing device with a maximum testing force 100 kN at the strain rate of $0.033\,s^{-1}$. Obtained records were used for the evaluation of the deformation behaviour and energy absorption ability of foam. Energy absorption ability was calculated from the region under the load-deflection curve, and the plateau length was determined in the region of the last stress drop in the area next to densification part [7].

3. Results and discussion

As shown in Fig. 1 and Fig. 2, a variation of the chemical composition (AA6061 and AA7075) results in significant differences in porous structure as pore size distribution, shape factor, the thickness of the surface skin and different thickness of the cell walls. The foam structure of AA6061 (Fig. 1) possesses a number of almost the same pores in comparison with AA7075 (small pores below 0.5 mm were rejected). However, the pores are larger with lower shape factor (0.6 to 0.9) and are inhomogeneously distributed within the structure. It is possible to observe more big pores close to the surface skin. Often clustering of larger pores takes place. Drainage of metal on the bottom of the AA6061 specimen is also characteristic. AA7075 foam mostly consists of small pores, which

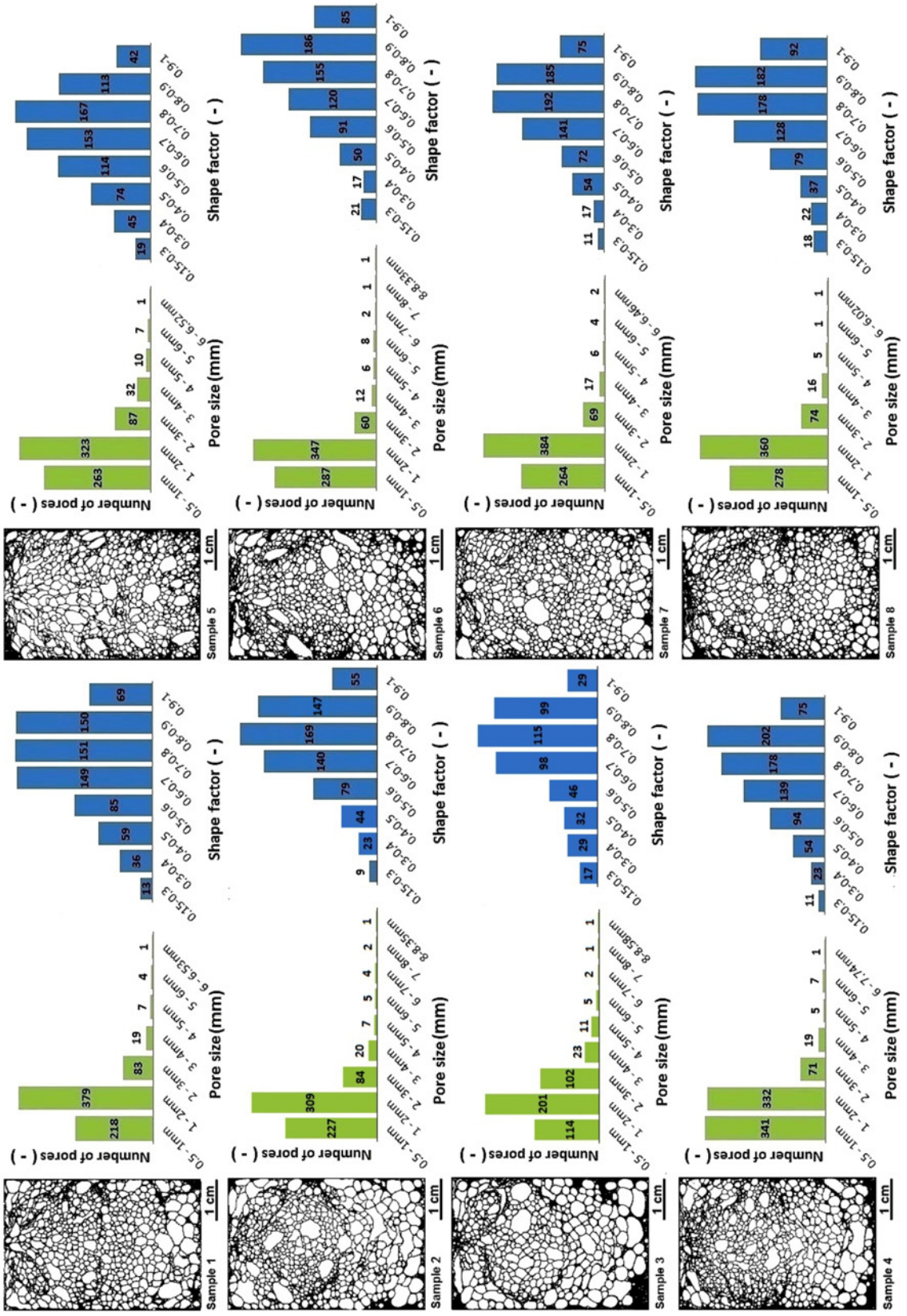

Fig. 1. Inner structures of tested samples AA6061 (1–4) and AA7075 (5–8) with calculated pore size and shape factor (3D tomography + Image J).

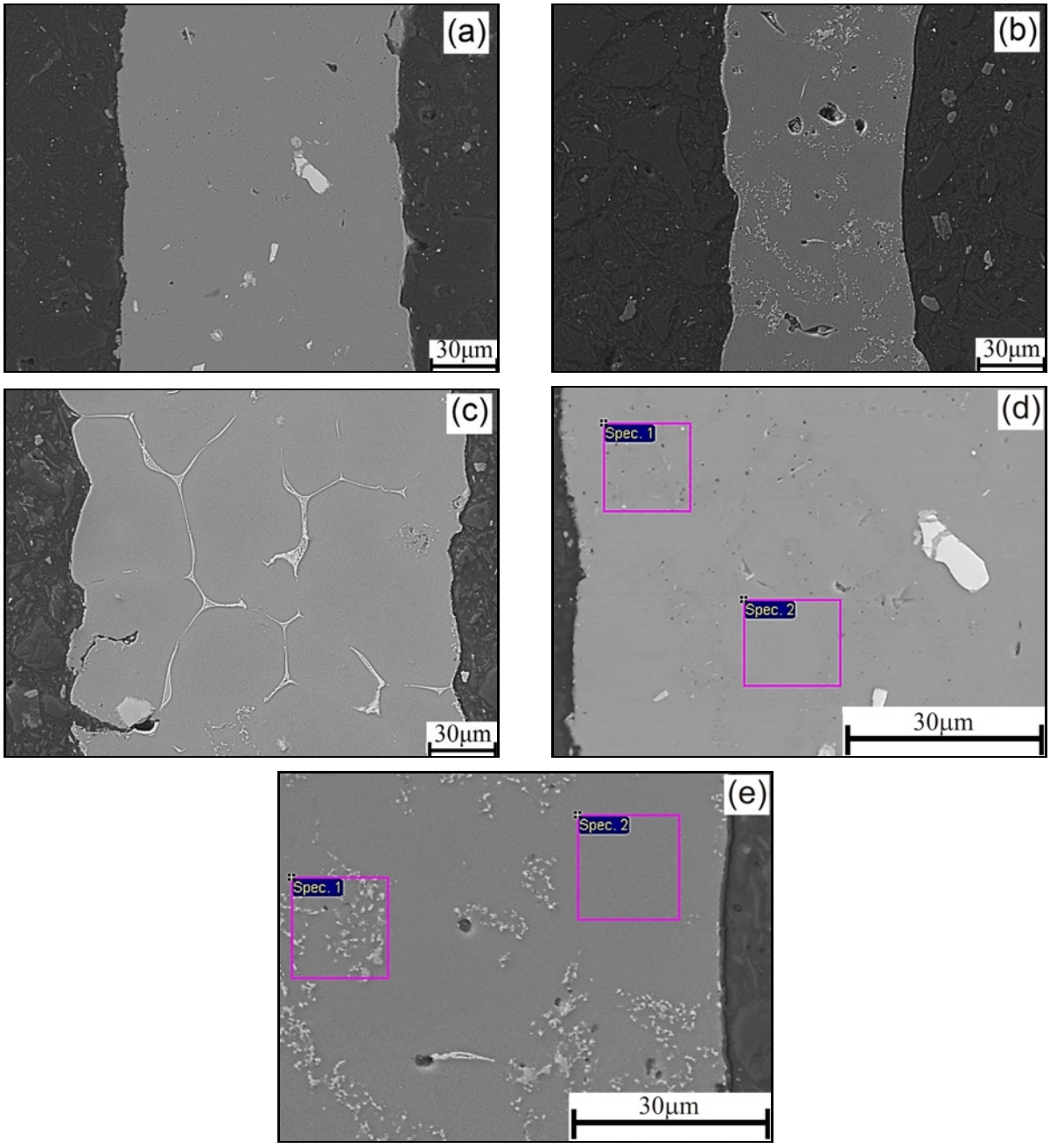

Fig. 2. Typical cell wall cross-section of (a) AA606, and (b) AA7075 from the middle of the sample, (c) from the bottom of the sample AA7075, EDS analyses of cell walls for (d) AA6061 and for (e) AA7075 (SEM).

are distributed rather uniformly with occasional occurrence of large pores usually surrounded by small pores (Fig. 1). The shape factor of the pores, in this case, is in the range of 0.7 to 1.0. The higher thickness of the surface skin of value 0.31–0.6 mm for up/down half part of the sample is observed for AA6061 foam. In the case of AA7075, the thickness of surface skin is about 0.25–0.4 mm without any significant variations between upper and lower part of the sample. The average pore diameter estimated for the observed structures in the vicinity of surface skin for AA6061 is 2.6 mm and 1.1 mm for AA7075.

The differences within the foam structure in dependence on the chemical composition can be attributed to different melting points of used elementary powders and aluminium alloys prepared by PM, especially for low melting elements (Zn) and different wt.% of AlMg5: 20 wt.% in case of AA6061 and 50 wt.% for AA7075. According to Standard EN 18273, the melting range of AlMg5 (AA5356) is between 562–633 °C. In regions with higher content of AlMg5, nucleation started earlier, and higher amount of H_2 was released than in a region with higher content of pure Al which results in variability of semi-solid state temperature

during early-foaming stages. Therefore, AA6061 contains biggest pores. AA7075 contains a higher amount of AlMg5 and therefore contains lower size pores. Inhomogeneities of chemical composition in foamable precursor and used elementary powders with different melting points are responsible for avoiding pore coalescence in early foaming stages for AA7075. In the case of low melting elements, the amount of released H_2 is also responsible for the shape of pores and their size [14, 15, 17, 18, 20, 25, 26]. Therefore, the formation of the higher amount of the smaller pores in space and close to the surface skin as shown in Fig. 1 is characteristic for AA7075 alloy due to appropriate synchronisation of the melting point of the alloy with starting decomposition temperature of the TiH_2 (400 °C) [27–29] and the creation of more defects in cell walls (Fig. 2). In the case of AA6061, there are observed rather large pores close to the surface skin (Fig. 1) in space due to the higher difference between the melting point of the alloy and decomposition temperature of the TiH_2. These large pores could negatively influence reproducibility of the compression stress after heat treatment since the foam becomes brittle [18]. As revealed in Fig. 2a, cell walls in case of AA6061 are thicker and contain fewer voids and microcorrugations in comparison with the microstructure of cell walls for AA7075. In both studied alloys are observed inhomogeneities of chemical composition. EDS analyses confirm (Fig. 2b) these inhomogeneities: for the content of Mg in the case of AA6061 is observed different chemical composition (Fig. 2d) between Spectrum 1 where was its amount 2 wt.% in comparison with Spectrum 2 (0.74 wt.% Mg). In areas with higher content of Mg, micropores are observed as a result of solidification process. The microstructure of AA7075 (Fig. 2e) also shows differences in chemical composition between Spectrum 1 where was Mg (4.6 wt.%) and Cu (4.5 wt.%) and Zn (8.5 wt.%) in comparison with Spectrum 2 where content of elements was following: Mg (1.8 wt.%), Cu (1.2 wt.%) and Zn (6.95 wt.%). These inhomogeneities of chemical composition resulted in different hardness (creation of precipitation phases) and led to the creation of voids within cell walls. Also in the case of AA7075 is observed drainage of Zn to the bottom of the sample (Fig. 2c).

Generally, the compression stress-strain curve is divided into three stages according to [9, 14–16, 30]. *The quasi-elastic stage* is characterised by an elastic deformation of the cell walls. The cracks, which are presented in the cell walls, are step by step closed by increasing compression stress [8]. *Plateau stage* is characterised by a deformation at almost constant stress level, stepwise compression of individual pore layers. At *densification stage* is foam structure compacted in whole sample volume [31–33, 24]. As seen in Fig. 3, the chemical composition of used alloys, the different inner porous structure at the constant density and heat

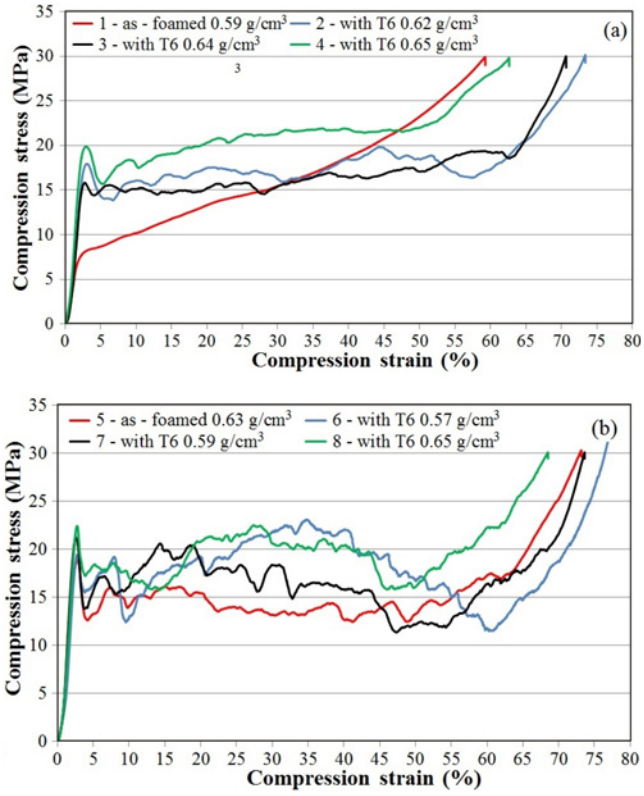

Fig. 3. Compression stress vs. strain curves of (a) AA6061 and (b) AA7075 alloy with numbers corresponding to images of the porous structure showed in Fig. 1 and Table 1.

treatment are responsible for the increase in the compression stress and changes in deformation behaviour, which are significant in the case of AA6061 and rather negligible in the case of AA7075. Reproducibility is enhanced in the case of AA7075. As-foamed AA6061 behaves in a typical ductile manner [18] which is characteristic by increasing stress with deformation, compression stress (CS) is 7.14 MPa, and no drop stress (DS) is observed as documented in Fig. 3a and Table 1. AA7075 foam behaves in a brittle manner as seen in Fig. 3b with typical stress drop down to 12.61 MPa after compression stress (18.89 MPa), followed by characteristic oscillation around plateau value prior steep increase of the stress during densification. However, after T6, there is observed the typical brittle manner of the stress-strain curve for both, AA6061 and AA7075 [10, 11], more inhomogeneous deformation in plateau region is observed for AA7075 (Fig. 3b). Differences between compression stresses after T6 are significantly lower when we compare foams of various chemical compositions, 17.5 ± 2.5 MPa for AA6061 and 21 ± 0.5 MPa for AA7075. Moreover, no significant differences in drop stress (DS) and strain at DS in dependence on chemical composition occur after T6, drop stress in % of CS for AA6061 is approximately 22 % and for AA7075 24 %, strain at drop stress is 5 %

Table 1. List of measured and calculated values: CS – compression stress, DS – drop stress, Δ strain is the strain difference between strain at DS and strain at CS, and calculated values of absorbed deformation energy up to 15, 30 and 55 % stress, and length of plateau at constant density 0.65 g cm^{-3}

Alloy	Sample	Density (g cm^{-3})	CS (MPa)	Strain at CS (%)	DS (MPa)	Δ strain (%)	Absorbed volume up to 15 %/30 %/55 % stress (kJ m^{-3})	Length of plateau (volume energy at end of plateau) (%) (kJ m^{-3})
AA6061	1 (T0)	0.59	7.14	1.91	–	–	175	35 (109)
	2 (T6)	0.62	17.95	3.11	13.84	3.62	67/148/291	58 (307)
	3 (T6)	0.64	15.82	2.78	14.41	1.35	65/137/271	63 (319)
	4 (T6)	0.65	19.86	2.97	15.69	2.22	78/176/350	55 (350)
AA7075	5 (T0)	0.63	18.89	2.79	12.61	1.44	66/135/243	62 (280)
	6 (T6)	0.57	19.41	2.77	15.50	1.04	70/162/319	70 (388)
	7 (T6)	0.59	21.23	2.58	13.79	1.16	75/162/278	68 (346)
	8 (T6)	0.65	22.43	2.73	17.22	1.15	76/174/324	64 (385)

for AA6061 and 3.9 % for AA7075. This indicates that the amplitude changes of stress-strain curves are due to changes in cell walls microstructure. The character of stress-strain curves seems to be identical as no changes of pore structure are observed after T6.

Besides the effect of material composition, subsequent heat treatment, and porous structure, we assume that hardness of cell walls, inhomogeneity within cell walls, their thickness, and thickness of the surface skin are also responsible for variation in strength, deformation behaviour of the foam and reproducibility of the mechanical properties. To confirm this, microhardness of cell walls was measured. In the case of AA6061, the hardness HV of the cell walls increases from 88.74 in the case of T0 up to 119.67, in the case of T6 and for AA7075, it is 104.24 before and 158.65 after T6. Therefore, there is approximately a 2.5× increase in the compression stress in the case of AA6061 observed. Heat treatment in case of AA7075 did not result in significant increase of the compression stress 0.11× due to the high concentration of defects within cell walls. However, an increase in hardness results in plateau value increase, and therefore, in the higher amount of the absorbed energy (Fig. 3b and Table 1) after T6. A higher value of absorbed energy in the case of AA7075 results from higher compression stress in plateau region and length of plateau itself. As described previously in several studies [9–12, 14, 15, 20, 21, 30], the crushing of the first pore band which contains innate defects in cell walls (mostly voids or microcracks) is responsible for stress drop following by densification of this pore band or weakest link while crushing of the other bands in different place within the foam volume occurs [9–12, 14, 15, 20, 30]. Therefore, thicker cell walls and surface skin are responsible for lower drop stress value (AA6061) since the role of inner voids in crushing process in the case of thicker cell walls is suppressed. Vice versa, if cell walls are thinner (AA7075), pores are smaller and contain more defects within, their effect is significant, and stress drop is higher and steep; whole and larger weak bands crush at once through the cross-section. More homogeneous distribution of the small pores within the volume with inherent defects in cell walls results in higher reproducibility in the case of AA7075, since there is no significant "weak area" within the structure as large pores with broken walls and crushing occur randomly. In a foam volume, a whole weak band of larger pores crush at once through the cross-section [11].

In comparison with previous research [10, 11, 17, 23] aluminium foam prepared with comparable chemical composition could have little differences in mechanical properties. The differences are due to various technological parameters and parameters of testing such as foaming temperature, heat treatment, strain rate, etc. Tested samples made of AA6061 without heat treatment reached lowest compression stress in comparison with previous research [10, 23]. After heat treatment, tested samples reached the same compression stress and deformation behaviour, even when different parameters were used for heat treatment T6 (water quenching).

As examined in previous research, compression stress of aluminium foam is also increased by using pre-treated TiH_2 [17, 18]. Thus prepared aluminium foam (AA6061) has a rather homogeneous distribution of small pores within the spatial, thicker cell walls in comparison to AA6061 (in comparison with samples prepared with as-received TiH_2) [18] and also with AA7075. That results in an increase in compression stress and reproducibility of the mechanical properties up to 23 ± 0.5 MPa (in comparison with samples AA7075 prepared with as-received TiH_2 21 ± 0.5 MPa). Tested samples made of AA7075 without heat treatment reached highest compression stress in comparison with previous research results [11, 23],

and deformation behaviour was rough with the strong disintegration of tested samples during loading. In the case of AA7075 was used different heat-treatment [11, 23] which had an influence on the creation of precipitation phases. The hardness of the material is important for compression strength, defects present in cell wall have a negative influence on compression strength and deformation behaviour in the case of AA7075.

Moreover, this observation confirms our assumption that the small pores with thin surface skin are responsible for an increase of the reproducibility of the compression strength of aluminium foam due to the strong effect of the inherent defects in the cell walls during the onset of deformation. Therefore, an AA6061 aluminium foam prepared with pre-treated TiH_2 has a shorter plateau with increased absorption ability and without strongest disintegration of the tested samples in comparison with samples AA7075 prepared with as-received TiH_2, and deformation curve can also be significantly affected by the precursor distribution itself [8].

From the above mentioned it can be clearly concluded, that the stress-strain curve can be simply adapted to application demands for certain porosity regarding strength, deformation energy and reproducibility by adjusting the composition of the metal alloy and additional heat treatment.

4. Conclusions

The effects of chemical composition (AA6061 and AA7075) and heat treatment on the PM aluminium foam structure and cell wall microstructure, their effects on the deformation behaviour and energy absorption ability with respect to adaptation of the deformation behaviour of the aluminium foam to industrial application demands were studied.

– It was confirmed that PM aluminium alloy composition strongly affects the stress-strain behaviour of aluminium foam at given density by affecting the early stage of the foaming and thus final porous structure.

– Increased hardness by heat treatment of the cell walls of aluminium foam significantly influences the strength of AA6061 foam (120–180 % increase of compression stress from T0 to T6) and has only small effect in the case of AA7075 foam (2.5–18.5 % increase of compression stress from T0 to T6).

– However, the energy absorption ability of the AA7075 foam is also increased in the case of heat treatment/increased hardness.

– Thinner cell walls with inherent defects within cell walls result in increased reproducibility of the strength of aluminium foam as can be seen in the case of AA7075 foam.

– Change of cell wall microstructure during T6 leads to changes in the hardness of cell wall material.

– In the case of AA7075 defects present in cell walls rule stress behaviour of this foam predominantly.

Findings in this study in hand with an effect of the pre-treatment of TiH_2 prior manufacturing of the foamable precursor and the proper positioning of the precursor within the mould before foaming can be successfully used for adaptation of the stress-strain curve of aluminium foams for application demands.

Acknowledgements

This work was supported by the Slovak Research and Development Agency under APVV contracts No. 0647-10 “ULTRALIGHT”, No. 0736-07 “LOWCOSTFOAM” and No. APVV-0692-12 “PCMPANEL”.

References

[1] Gibson, L. J., Ashby, M. F.: Cellular Solids: Structure and Properties. Cambridge, Cambridge University Press 1997.
[2] Ashby, M. F., Evans, A., Fleck, N. A., Gibson, L. J., Hutchinson, J. W., Wadley, H. N. G.: Metal Foams – A Design Guide. Boston, Butterworth-Heinemann 2000.
[3] Banhart, J.: Prog Mater Sci, *46*, 2001, p. 559. doi:10.1016/S0079-6425(00)00002-5
[4] Florek, R., Simančík, F., Harnúšková, J., Orovčík, Ľ.: Proc Mater Sci, *4*, 2014, p. 323. doi:10.1016/j.mspro.2014.07.566
[5] Simančík, F., Banhart, J., Ashby, M. F., Fleck, N. A.: Metal Foam and Porous Metal Structure. Bremen, MIT-Verlag 1999.
[6] Evan, A. G., Hutchinson, J. W., Ashby, M. F.: Prog Mater Sci, *43*, 1998, p. 171. doi:10.1016/S0079-6425(98)00004-8
[7] Florek, R., Simančík, F., Nosko, M., Harnúšková, J.: Powder Metallurgy Progress, *10*, 2010, p. 207.
[8] Nosko, M., Simančík, F., Florek, R.: Mater Sci Eng A, *527*, 2010, p. 5900. doi:10.1016/j.msea.2010.05.073
[9] Garcia-Moreno, F.: Materials, *9*, 2016, p. 1. doi:10.3390/ma9020085
[10] Lehmhus, D., Banhart, J.: Mater Sci Eng A, *349*, 2003, p. 98. doi:10.1016/S0921-5093(02)00582-8
[11] Campana, F., Pilone, D.: Scripta Mater, *60*, 2009, p. 679. doi:10.1016/j.scriptamat.2008.12.045
[12] Mu, Y., Yao, G., Liang, L., Luo, H., Zu, G.: Scripta Mater, *63*, 2010, p. 629. doi:10.1016/j.scriptamat.2010.05.041
[13] Wang, Z., Li, Z., Ning, J., Zhao, L.: Mater Design, *30*, 2009, p. 977. doi:10.1016/j.matdes.2008.06.058
[14] Ramamurty, U., Paul, A.: Acta Mater, *52*, 2004, p. 869. doi:10.1016/j.actamat.2003.10.021
[15] Koza, E., Leonowicz, M., Wojciechowski, S., Simančík, F.: Mater Lett, *58*, 2003, p. 132. doi:10.1016/S0167-577X(03)00430-0
[16] Helfen, L., Baumbach, T., Stanzick, H., Banhart, J.: Adv Eng Mater, *4*, 2002, p. 808. doi:10.1002/1527-2648(20021014)4:10<808::AID-ADEM808>3.0.CO;2-U

[17] Lehmhus, D., Busse, M.: Matwiss Werkstofftech, *45*, 2014, p. 1049. doi:10.1002/mawe.201470120
[18] Orovčík, Ľ., Nosko, M., Švec Sr., P., Nagy, Š., Čavojský, M., Simančík, F., Jerz, J.: Mater Lett, *148*, 2015, p. 82. doi:10.1016/j.matlet.2015.02.062
[19] Duarte, I., Oliveira, M., Garcia-Moreno, F.: Colloids Surfaces A, *438*, 2013, p. 47. doi:10.1016/j.colsurfa.2013.02.061
[20] Garcia-Moreno, F., Fromme, M.: Cellular Metals. Berlin, MIT-Verlag 2003.
[21] Marsavina, L., Kováčik, J., Linul, E.: Theor Appl Fract Mec, *83*, 2016, p. 11. doi:10.1016/j.tafmec.2015.12.020
[22] Duarte, I., Banhart, J.: Acta Mater, *48*, 2000, p. 2349. doi:10.1016/S1359-6454(00)00020-3
[23] Lehmhus, D., Banhart, J., Rodriguez-Perez, M. A.: Mater Sci Technol, *18*, 2002, p. 474. doi:10.1179/026708302225002182
[24] Reglero, J. A., Solórzano, E., Rodríguez-Pérez, M. A., De Saja, J. A., Porras, E.: Mater Design, *31*, 2010, p. 3568. doi:10.1016/j.matdes.2010.02.025
[25] Körner, C., Berger, F., Arnold, M., Stadelmann, C., Singer, R. F.: Mater Sci Technol, *16*, 2000, p. 781. doi:10.1179/026708300101508432
[26] Saadatfar, M., Mukherjee, M., Madadi, M., Schröder-Turk, G. E., Garcia-Moreno, F., Schaller, F. M., Hutzler, S., Sheppard, A. P., Banhart, J., Ramamurty, U.: Acta Mater, *60*, 2012, p. 3604. doi:10.1016/j.actamat.2012.02.029
[27] Matijasevic-Lux, B., Banhart, J.: Scripta Mater, *54*, 2006, p. 503. doi:10.1016/j.scriptamat.2005.10.045
[28] Matijasevic-Lux, B., Banhart, J., Fiechter, S., Görke, O., Wanderka, N.: Acta Mater, *54*, 2006, p. 1887. doi:10.1016/j.actamat.2005.12.012
[29] Mandrino, D., Paulin, I., Škapin, S. D.: Mater Charact, *72*, 2012, p. 87. doi:10.1016/j.matchar.2012.07.005
[30] Mukherjee, M., Kolluri, M., Garcia-Moreno, F., Banhart, J., Ramamurty, U.: Scripta Mater, *61*, 2009, p. 752. doi:10.1016/j.scriptamat.2009.06.023
[31] Bastawros, A. F., Bart-Smith, H., Evans, A. G.: Mech Phys Solids, *48*, 2000, p. 301. doi:10.1016/S0022-5096(99)00035-6
[32] Kolluri, M., Mukherjee, M., Garcia-Moreno, F., Banhart, J., Ramamurty, U.: Acta Mater, *56*, 2008, p. 1114. doi:10.1016/j.actamat.2007.11.004
[33] Kumar, P. S., Ramachandra, S., Ramamurty, U.: Mater Sci Eng A, *347*, 2003, p. 330. doi:10.1016/S0921-5093(02)00608-1